High-Frequency B-Mode Ultrasound for the Measurement of Intracranial Motion in Head Rotation

Ann Mallory, Yun-Seok Kang, Rod Herriott,
Heather Rhule, Bruce Donnelly, Kevin Moorhouse

ABSTRACT

The immediate goal of this research effort was to develop experimental methods to image and quantify the relative motion of the meninges and peripheral brain during head motion. Specifically, B-mode ultrasound was used to image these tissues in post-mortem human subject heads during anterior-posterior rotation testing. These procedures are needed to better understand the mechanism of peripheral injuries such as subdural hematoma and to quantify how human injury risk in head rotation varies with brain atrophy. In low-rate rotation testing, high-frequency B-mode ultrasound was successful in tracking the relative motion of the dura and underlying tissues. Images collected during high-rate rotation testing suggested that B-mode ultrasound has the potential to capture relative meningeal motion in trauma-level head rotation tests if outward bulging of the tissues and resulting out-of-plane motion can be reduced. Preliminary efforts to eliminate out-of-plane motion by mounting the ultrasound transducer to the structure that rotates with the head have been promising.

INTRODUCTION

Subdural hematoma is a frequent and life-threatening injury, especially for the elderly (Gennarelli et al., 2005, Sawauchi et al., 2008, Stitzel et al., 2008, Taussky et al., 2008, Hanif et al., 2009, Perel et al., 2009, Mallory, 2010). Although previous autopsy and surgical epidemiology studies have attributed a large proportion of subdural hematomas to brain contusions or ruptured vessels on the surface of the brain (Jamieson et al., 1972, Maxeiner, 1997, Maxeiner et al., 2002), analysis of motor vehicle crash data suggests that subdural hematomas originating with bleeding from the bridging veins that cross the meninges and empty into the dural sinuses are more frequent among older motor vehicle crash occupants (Mallory et al., 2011). This increasing frequency of bridging-vein sourced subdural hematomas with age, along with

epidemiological data on the overall increase in the frequency and poor outcome of subdural hematoma in the elderly, supports that estimation of subdural injury risk will require understanding the increasing risk of bridging-vein subdural hematomas as a function of age.

Subdural hematomas associated with bridging vein damage are believed to result from stretching the veins to failure with motion of the brain relative to the skull during head rotation (Holbourn, 1943). Experimental models using human cadavers (Löwenhielm, 1974, Depreitere et al., 2006) and primates (Ommaya et al., 1968, Gennarelli et al., 1982, Ommaya et al., 2002) have successfully produced bridging vein tears with head rotation. Brain atrophy is thought to contribute to bridging vein tears in older trauma patients based on the assumption that increased atrophy can lead to increased motion of the brain relative to the skull resulting in tension in the bridging veins (Yamashima et al., 1984, Meaney, 1991, Kleiven et al., 2002, Hanif et al., 2009).

Since bridging veins cross from the surface of the brain through the arachnoid and dura into the dural sinuses, it is the motion of these layers that would be expected to determine the magnitude of bridging vein stretch during head motion and the risk of bleeding into the layers between these meningeal tissues. Therefore, understanding the relationship between brain atrophy and relative brain motion during head rotation is essential to improve understanding of the mechanism of subdural hematoma and to define injury risk as a function of age. Since the age-related increase in subdural hematomas associated with suspected bridging vein failure in motor vehicle crashes was most notable with anterior-posterior head motion in frontal crashes (Mallory et al., 2011), anterior-posterior head rotation is of particular interest.

Experimentally, motion at the surface of the brain has been previously explored using a number of methods. In live primate testing and in post-mortem piglet testing, researchers have tracked motion of parts of the brain relative to the skull by visually recording it through transparent viewing windows that have replaced parts of the skull or brain (Sheldon et al., 1944, Pudenz et al., 1946, Gosch et al., 1970, Ibrahim et al., 2010). However, removal of the boundary layers and damage to the adjacent meningeal structures limited conclusions that could be made regarding motion of the peripheral structures. Radiography studies used radio-opaque markers and intravascular contrast fluid introduced into the brain (Hodgson et al., 1966, Sass et al., 1971, Shatsky et al., 1974, Stalnaker et al., 1977, Nusholtz et al., 1984, Hardy et al., 2007) to track motion. However, even those that imaged motion *near* the surface of the brain lacked the resolution to differentiate motion of the meningeal layers from deformation deeper in the cortex. Many of the radiology studies were also invasive, breaching the peripheral tissues of interest to place radiopaque materials deeper in the brain. Human volunteer studies with magnetic resonance (MR) imaging have come closer to imaging motion near the surface of the brain in the cortex, but could not distinguish meningeal layers or be used for high-rate testing (Ji et al., 2004, Bayly et al., 2005, Sabet et al., 2008, Feng et al., 2010). Other novel efforts to track brain motion have included the implantation of accelerometers (Trosseille et al., 1992, King et al., 1995) and the insertion of fine wires to make fine tears in the brain tissue to show the extent of displacement (Viano et al., 1997). Although all of these innovative efforts have revealed information about relative motion of the brain within the head, none have been focused on non-invasively measuring the motion relative to the skull of both the cortical surface and the meninges in high-rate rotation.

Physical and computational models have been inconsistent in predicting motion near the surface of the brain because of the variety of brain-skull interface definitions used. Models with boundary interfaces between the brain and skull have been reported across a spectrum of interface connections from sliding or full-slip to tied or no-slip. Yet in spite of these major differences in boundary conditions, models with full-slip brain-skull interfaces and models with no-slip brain-skull interfaces have been successfully validated against motion data deep in the brain, supporting Margulies' conclusion that the influence of the skull-brain interface is attenuated for locations central in the brain (Margulies et al., 1990). As a result, it is unclear how the motion at the surface of the brain can be predicted using physical or computational models in the absence of supporting experimental data specifically documenting motion of these tissues.

Therefore, a new method of measuring peripheral brain and tissue motion during high-rate rotation is needed to better understand the mechanism and risk of bridging vein subdural hematomas across age groups, but also to validate and improve computational models of peripheral brain motion. Among non-invasive imaging methods, ultrasound offers the potential for high-resolution images collected at high frame-

rates. Previously, ultrafast ultrasound technology has been used to observe the deformation of the kidney during isolated compression testing (Helfenstein-Didier et al., 2015), as well as the response of the colon and liver in whole-body post-mortem impacts (Beillas et al., 2013).

This workshop paper describes the work in progress to develop methods to experimentally track the motion of the cortical surface and the meningeal tissues relative to the skull during experimental head rotation testing of post-mortem human subjects using B-mode ("brightness" mode) ultrasound. B-mode ultrasound is limited to slower frame-rates than the ultrafast ultrasonography used previously in abdominal testing but capable of finer spatial resolution, offering the potential to image the individual layers of the meninges and cortical surface.

METHODS

B-mode ultrasound imaging of peripheral brain tissues was performed during rotation testing of two post-mortem human subject heads. The post-mortem heads were mounted on a rotating frame that moved the head past a stationary ultrasound probe so that the meningeal tissues could be imaged during head rotation through a parasagittal window in the skull. Methods are described for the preparation and testing of post-mortem heads, the design of the rotation fixture, and the collection and analysis of ultrasound images.

Post-Mortem Subject Preparation

Testing on post-mortem human subjects from the Ohio State University's Anatomy Body Donation Program was performed with the approval of the Ohio State University Institutional Review Board.

Initial preparation procedures included removal of the scalp to expose the cranial vault. Since rotation loading would be applied through the jaw as well as to the skull, alignment of dentition was confirmed and secured if necessary. The head and neck were disarticulated from the rest of the spine at C7-T1. Immediately following separation, the space between the spinal dura and arachnoid was plugged to prevent air seepage into the cranium. The plug, which consisted of layers of petroleum jelly and yarn coated in a 1:10 mixture of paraffin and petroleum jelly, was impermeable to air and fluid. The external carotids were ligated to reduce perfusion into the neck and scalp vessels when the arterial system was later pressurized. All exposed tissues at the neck were sealed using gel cyanoacrylate (Loctite 426 Instant Adhesive, Loctite, Henkel Corporation, Düsseldorf, Germany) and nylon panty hose.

Cranial Viewing Window. A parasagittal craniectomy exposed the dura along the anterior-posterior path to be imaged (Figure 1). On Subject 1, the opening was 25 mm wide and centered 35 mm from the mid-sagittal plane. On Subject 2, the opening was centered 31 mm from mid-sagittal and narrower than for Subject 1: the 19 mm wide opening was buttressed along the periphery with two-part epoxy (Wet Weld, JB Weld, Sulphur Springs, Texas) for an effective window width of approximately 10 mm. The opening was cut using a surgical craniotome and cutting blade with dura guard (Model 6516-01-378-A176, Aesculap, Center Valley, Pennsylvania). When the dura on Subject 1 was inadvertently cut during the craniectomy procedure, the tear was sutured and sealed with gel cyanoacrylate so that this opening in the skull could still be used for imaging. For Subject 2, after an initial attempt at a craniectomy on the left again resulted in a torn dura, craniectomy methods were modified to separate the dura from the skull with a Penfield surgical elevator for a successful craniectomy on the right side of the head. Following the craniectomy, the exposed dura was kept hydrated with artificial CSF and all testing was performed on the right side of the head.

Cerebrospinal Fluid (CSF) Perfusion. A Foley catheter was inserted into the posterior spinal subarachnoid space at the transected C7-T1 level in order to perfuse the cranial subarachnoid space with artificial CSF. Extreme care was taken to avoid any damage to the arachnoid which would allow the fluid to drain from the subarachnoid space into the layer between the dura and arachnoid. The artificial CSF, prepared with distilled water using the solution developed by Sugawara et al. (1996), was perfused at a fluid column pressure of approximately 40 mmHg over at least 20 hours prior to testing.
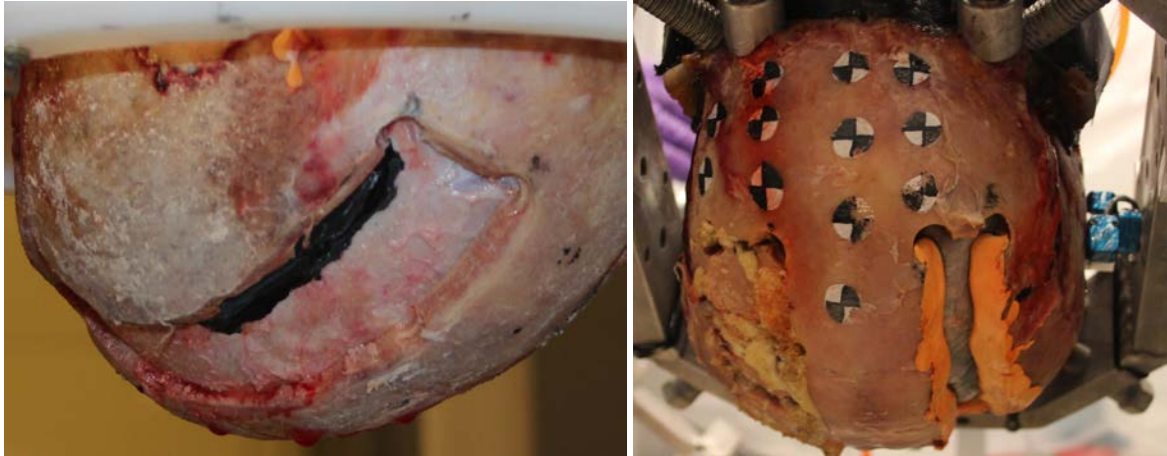
Figure 1. Parasagittal craniectomy Subject 1 (left) and Subject 2 (right)

Vascular Pressurization.   The primary goal of vascular pressurization was to produce physiologically-appropriate levels of intracranial pressure (ICP) since brain motion is expected to depend more directly on ICP than on applied venous or arterial pressure.   Preliminary trials with post-mortem subjects had shown that producing ICP in the normal physiological target range of 5-15 mmHg (Raboel et al., 2012) required much lower arterial and venous pressures than the normal range of in vivo blood pressure.

The cranial <u>arterial</u> system was pressurized with saline via the internal carotid arteries at the severed C7-T1 level.   Initially, the vertebral arteries were left open to flush the cranial arterial system at a nominal fluid pressure of 92 mmHg.   For testing, vertebral arteries were ligated and arterial input pressure was applied at nominal input pressures of 27 to 30 mmHg prior to testing.

The cranial <u>venous</u> system was pressurized with saline, tinted with Sunshine Orange RIT clothing dye (Quality Brands, Stamford, Connecticut) via the internal jugular veins at C7-T1.   Initial flushing was achieved by connecting each internal jugular vein individually at a nominal fluid pressure of 92 mmHg until tinted saline flowed from the other internal jugular.   For testing, venous input pressure was applied at nominal input pressures of approximately 45 mmHg prior to testing.

In Subject 1, pressurization was applied for 2 to 4 minutes prior to each rotation test.   In Subject 2, pressurization was applied for 15 seconds prior to each test.   Immediately prior to testing for both subjects, the arterial and venous pressurization systems were closed, effectively isolating the head from further pressurization during rotation testing.

Post-test pressure evaluation on each subject was performed by invasively measuring ICP with the vascular pressurization fluids applied at the same input pressure and duration as during testing.   In the post-test evaluation, a Codman Microsensor ICP Transducer (Codman & Shurtleff Inc. Rahnham Massachusetts) was inserted through the dura and into the parenchyma along the mid-pupillary line on the ultrasound-tested side of the head.   The head was placed in the start position used for rotation testing, and arterial, venous, and subarachnoid fluids were positioned at the same heights used for testing to reproduce the intracranial pressure attained during testing.

Rotation Test Fixture and Procedures

Head Rotation Fixture.   For anterior-to-posterior rotation testing the head was gripped in a rotating aluminum halo structure (Figure 2) using threaded locator bolts that positioned the head without penetrating the skull (Figure 3).   Threaded bolts were customized with rounded endpoints, except frontally where aluminum brow fittings were custom-made to engage the supraorbital ridge.   A chin-bar was adjustable for height and angle in order to fully engage the inferior surface of the mandible.
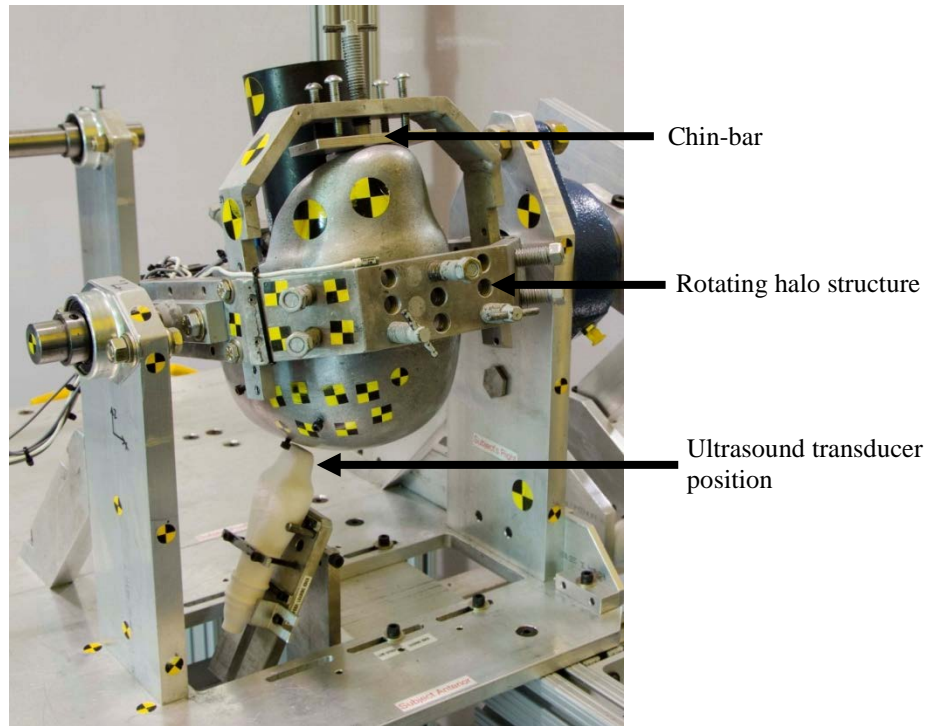
Figure 2. Shaft-mounted rotation fixture with halo structure to grip head, shown with dummy ultrasound transducer in place

Figure 3. Customized locator bolts to grip skull (left) and alternative bolt grips for engaging the supraorbital ridge (right)

The head was positioned so that the halo's axis of rotation was aligned through the center of curvature of the dural surface in the parasagittal window. This position allowed the surface of the dura to remain a constant distance from the stationary ultrasound probe throughout the arc of head rotation.

High-rate Rotation of the Head. In high-rate testing, the head and halo structure were accelerated by applying a linear force to the 11-cm load arm extending from the fixture's rotating shaft using a production passenger car seat-belt pretensioner (TRW 5F13-5461202-AAW, TRW, Livonia, Michigan) as shown in Figure 4. The pretensioner was mounted in a housing fit with custom-cut wood blocks for each test to limit stroke of the pretensioner as a method of controlling the energy applied. Since the stationary transducer could only clearly image motion up to speeds of 1.9 m/s with the image width used in the current testing, optimal stroke length for each subject was determined conservatively based on the radial distance of the imaged surface to the axis of rotation, the moment of inertia of each subject head in the rotating halo, and the empirically-estimated relationship between stroke length and energy for the model of pretensioners used.

Head rotation was slowed to a stop using a braking damper with a padded face against the 22 cm braking arm that extended from the shaft of the rotating fixture.
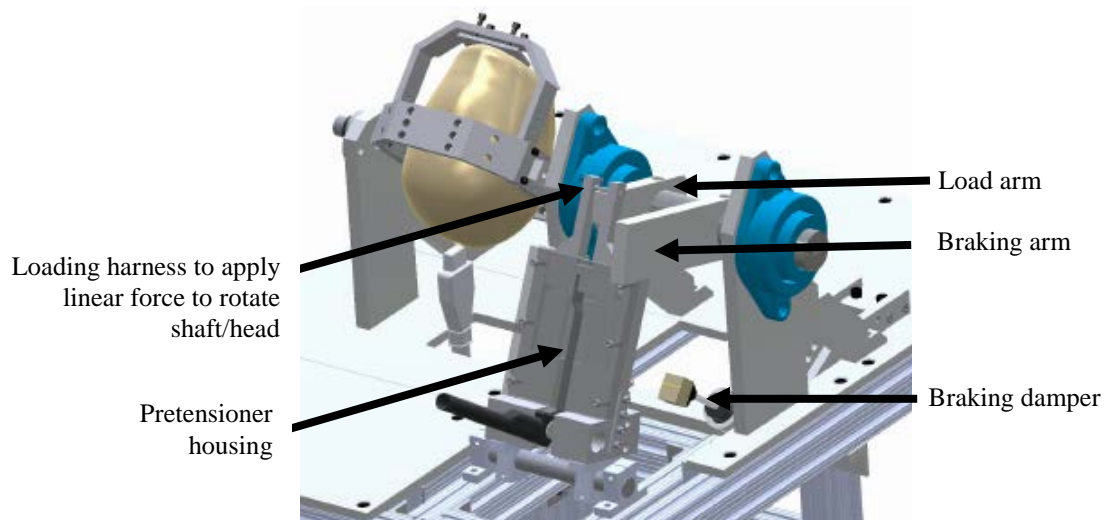
Figure 4. Head rotation pretensioner-powered acceleration fixture

Low-rate Rotation of the Head. In low-rate loading, the rotation shaft was accelerated from rest by gravity, then brought to a stop using a padded brake-stop for the 22 cm braking-arm. For Subject 1, the motion was in an anterior-to-posterior direction so that deceleration simulated an occipital impact. For Subject 2, the motion was in a posterior-to-anterior direction so that deceleration simulated a frontal head impact. The targeted kinematic range for initial rotational velocity prior to deceleration was 2.05 to 2.20 rad/sec. Target peak rotational deceleration during the simulated "impact" was 124 to 143 rad/sec^2. This deceleration pulse has been applied to volunteers without causing injury (Feng et al., 2010) and was not expected to result in damage or injury to the post-mortem subjects.

Kinematic Instrumentation of the Head and Halo. The Y-axis of the fixture-based coordinate system corresponded to the axis of rotation of the rotation fixture. The rotation shaft and both sides of the halo structure were instrumented with angular rate sensors (ARS PRO-18K, DTS, Seal Beach, California, USA) to track rotational velocity about the Y-axis. Three orthogonally-mounted angular rate sensors (ARS-18K, DTS, Seal Beach, CA, USA) were mounted to the skull, located to avoid submersion in ultrasound fluid medium. Endevco 7264 uniaxial accelerometers (Meggitt Sensing Systems, San Juan Capistrano, California) were mounted on the anterior and posterior halo to calculate rotational acceleration about the Y-axis.

Acceleration and rotational velocity results were processed by removing offset prior to motion and filtering with a low-pass CFC 180 filter (300 Hz) using DIAdem Version 12 (National Instruments, Austin, Texas). Head rotational velocity, measured using skull-mounted orthogonal angular rate sensors, were transformed to the fixture co-ordinate system to yield rotational velocity of the head about the fixture's Y-axis. Rotational acceleration of the rotation halo was estimated by dividing the difference between the output of two halo-mounted accelerometers by the distance between them. Head angle was estimated by integration of halo- and head-mounted angular rate sensors.

Ultrasound Imaging and Analysis

Ultrasound Imaging of Meningeal Tissues. High-speed, high-frequency ultrasound images were collected using a Vevo 2100 imaging system (VisualSonics Inc., Toronto, Ontario, Canada) with a 550D probe at a sound wave center frequency of 40 MHz, much higher than typical clinically-used frequencies of 2 to 20 MHz. The image frame width was 4.08 mm and the axial/vertical image height was 13 mm. The frame rate was 693 frames per second and the 1000-frame duration was sufficient to capture the entire motion sequence including acceleration and deceleration of the head in low-rate and high-rate rotation tests.

The ultrasound probe was mounted in a stationary position below the head, adjacent to the exposed dura in the parasagittal opening in the skull and aligned with the plane of rotation. The probe was oriented in a retrograde configuration, i.e. so that the firing sequence of the individual ultrasound crystals across the transducer array was in the *opposite* direction as the motion of the tissue relative to the probe.

Ultrasound Motion Analysis. Tissue tracking in video sequences of ultrasound images was performed using TEMA Version 3.7 image analysis software (Image Systems, Linköping, Sweden), with the image scaling factor determined using the VevoStrain post-processing utility for the Vevo 2100.

Points throughout the image, on the dura, arachnoid, and in the visible cortex, were tracked in the rotation test ultrasound images. The motion of these points was used to estimate the cumulative displacement of the arachnoid and cortex relative to the dura for each test. In B-mode ultrasound images, scan lines across the image are produced sequentially, as the ultrasound array sweeps from the leading side of the image to the trailing side of the image so that features on one side of the image frame are captured at a different point in time than features on the other side of the image frame. This sequential image-building leads to spatio-temporal distortion that is corrected by accounting for the true time at which each feature is captured in time-history tracking analysis. The sequential leading-side to trailing-side image building also results in differences in distortion for tissue moving in the *same* direction (prograde) versus the *opposite* direction (retrograde) as the transducer firing sequence. Higher speed tissue motion can be captured in a retrograde configuration than in a prograde configuration. The methods used for correction of the spatio-temporal distortion that results from sequential building of B-mode images are described in detail in Mallory (2014), along with the results of validation testing to confirm the accuracy of motion analysis using these correction and tracking methods.

For synchronization with kinematic data, time zero was identified by determining the time at which tissue motion was detected. Because B-mode ultrasound does not capture a strobe-type image, but builds the image sequentially, tissue motion can begin partway through the construction of a single image frame so that tissue on the trailing side of the frame appears to begin moving before tissue imaged on the leading side of the frame. Therefore, time zero was identified using the lateral position at which motion appeared to start in the first frame in which motion was visible, based on the premise that the time at which each point is imaged is proportional to its lateral position in the frame.

Since tissue moved past the ultrasound transducer like scenery viewed through a window in a moving vehicle, cumulative tissue motion of each tissue layer had to be calculated by stitching together the time-displacement histories of individual tissue points moving through the image window. The starting displacement of each tracked point was calculated by interpolation of the time-displacement history estimated for that layer from all previously tracked points. The previously-tracked points in each tissue layer (dura, arachnoid, layers of the cortex) were curve-fit using the Matlab weighted linear least-squares "loess" smoothing function, which uses local regression on a quadratic model.

The assumption that the dura was coupled with the skull during rotation was tested by comparing dura motion with skull motion for each test. Rotation angle of the head about the fixture's Y-axis was estimated from the dura time-displacement history by dividing the cumulative displacement of the dura by the radius of rotation (the distance from the fixture's rotation axis to the dura). The rotation angle time-history calculated from the ultrasound-tracked dura was then compared for each test to the head angle about the Y-axis calculated using the skull-mounted angular rate sensors.

Ultrasound Fluid Medium. Artificial CSF, prepared using degassed, distilled water was used as an imaging medium between the ultrasound transducer and the dural surface. The dural surface was submerged in a pan of the fluid, the base of which was fitted with a rubber baffle that allowed the ultrasound probe to stay dry when extended into place adjacent to the exposed dura surface in the craniectomy window (Figure 5). The baffle material was cut from a condom (Trojan Magnum, Church & Dwight, Annapolis, Maryland) that was empirically determined to minimize attenuation of ultrasound signal compared to other brands.
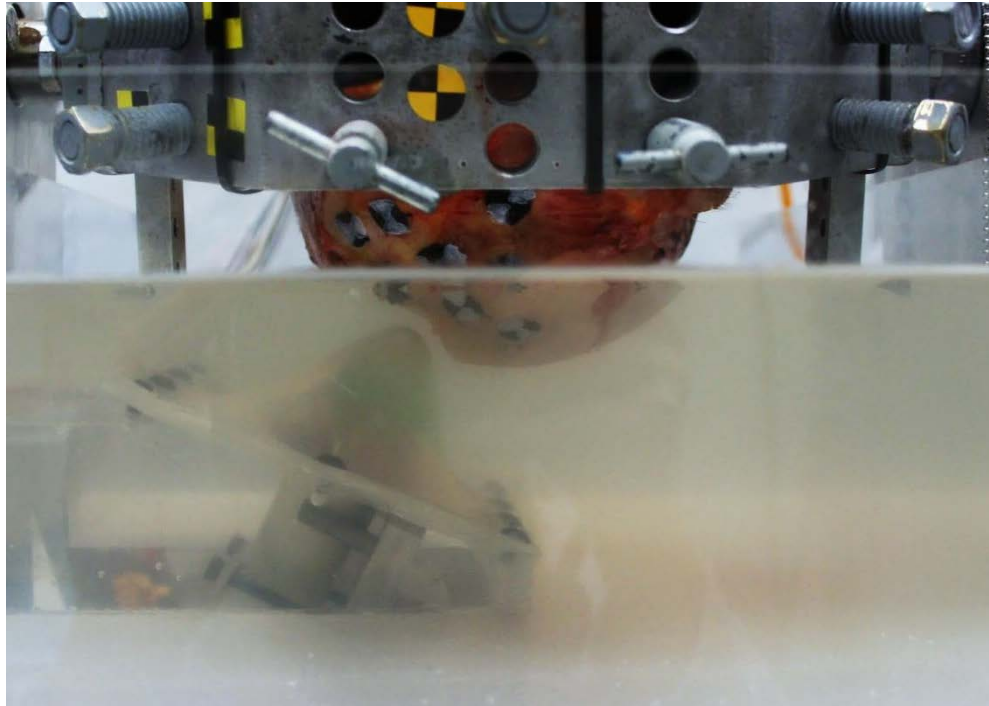
Figure 5. Ultrasound probe in position adjacent to submerged exposed dural surface (photographed through acrylic fluid pan)

Additional procedures performed on the subjects but not discussed in detail in this manuscript include MR imaging of the head for estimation of atrophy, determination of the center of curvature of the exposed dura, measurement of the mass moment of inertia of the head and rotating fixture, and 3-dimensional point digitization of the head and fixture. More detailed descriptions of all experimental procedures and image analysis methods used can be found in Mallory (2014).

RESULTS

Full rotation testing was performed on two post-mortem heads. Both subjects were female, with a cause of death of thoracic cancer. For both subjects, the radius of curvature along the dural surface in the craniectomy window was 8 cm, so that the head was positioned with the fixture shaft centered at a radial distance of 8 cm from the dural surface. Subject 1 was available for preparation 9.6 hours after death and testing was complete within 59 hours post-mortem. Subject 2 was available 29.5 hours after death and testing was complete by 86 hours. Subject characteristics are shown in Table 1.

Table 1. Post-mortem subject characteristics

Subject #	Age	Height	Weight	Head Width at Tragions	Mass Head and Neck
1	75	160 cm	83 kg	14.7 cm	4538 g
2	49	165 cm	67 kg	11.6 cm	3950 g

Subject 1

On Subject 1, the dura was damaged during craniectomy attempts on both the left and right sides of the head. The damaged dura in the opening on the left side of the head was repaired as described in the Methods section and testing and imaging proceeded on the left side of the head. However, in spite of repairing the torn dura, it appeared from ultrasound images that the fluid used as imaging medium had penetrated between the dura and arachnoid during test procedures (Figure 6). Therefore all motion analysis results presented in this manuscript are from Subject 2.
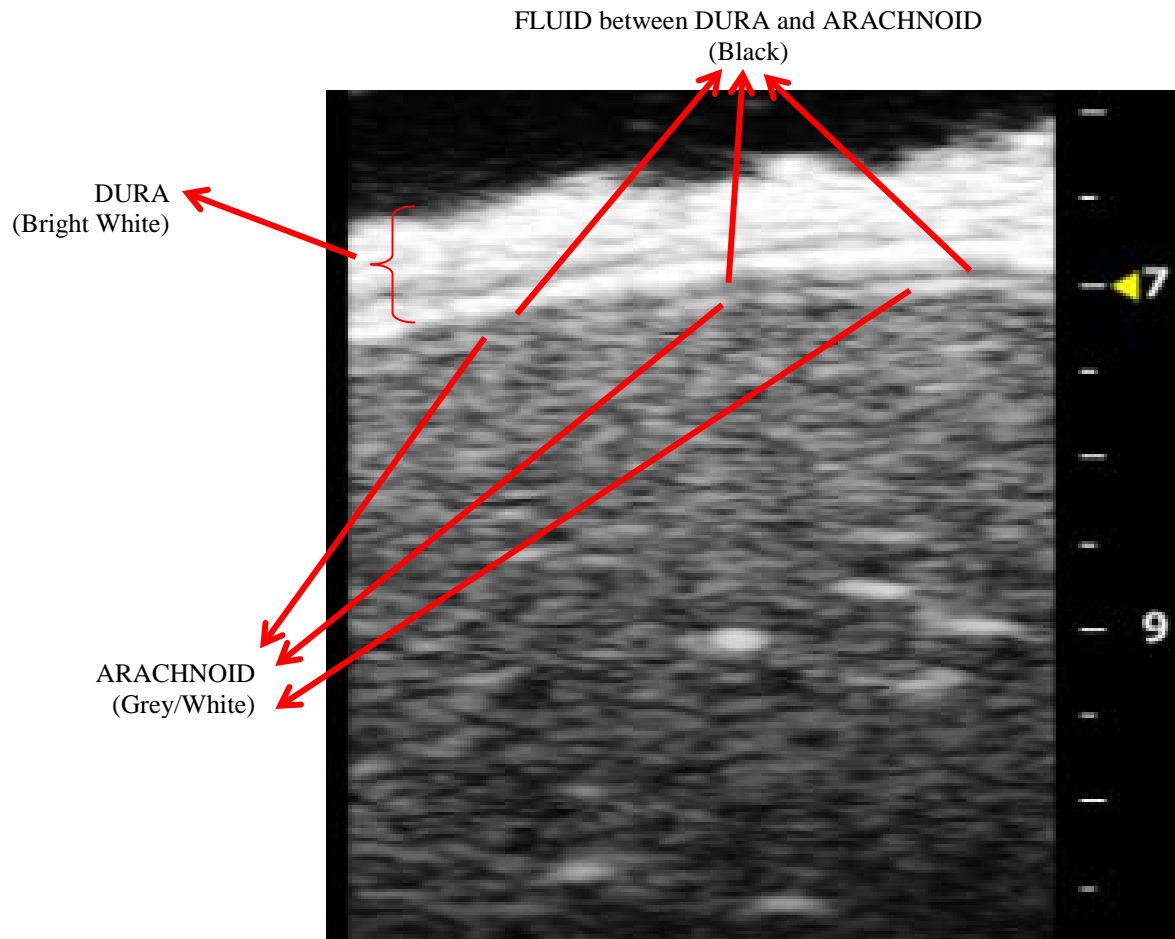
Figure 6. Ultrasound image frame from test subject 1 with fluid layer visible between dura and arachnoid (scale in mm on right indicates tissue depth from ultrasound array)

Subject 2

Low-rate Test Results. For Subject 2, initial ultrasound images were collected during seven low-rate tests. A sample ultrasound image (Figure 7) is shown for test LOW05, one of the four tests that were within the targeted ranges for rotational velocity at the moment of the simulated "impact" and peak deceleration during the deceleration phase. Rotational velocity for test LOW05 prior to deceleration was 2.18 rad/sec (125 deg/sec) and the deceleration pulse had a peak of 135 rad/sec^2 and a duration of approximately 50 msec.
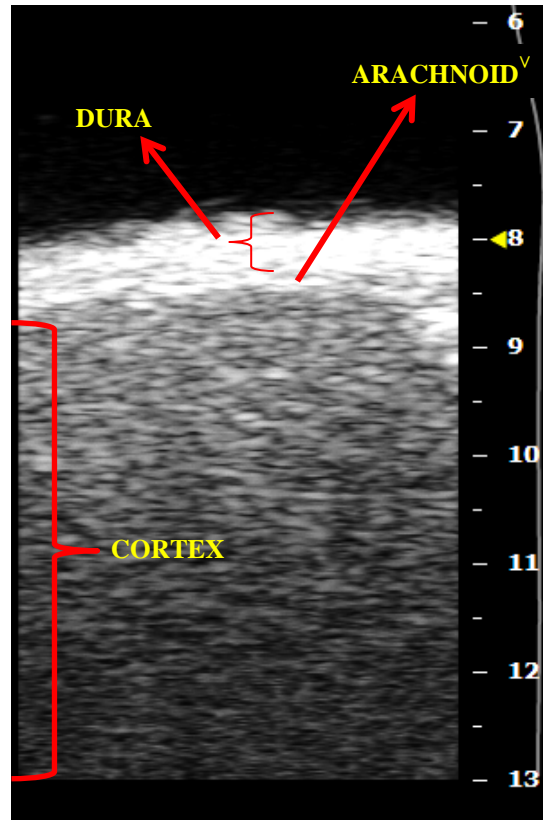
Figure 7. Image frame from Subject 2 (prior to motion)

In low-rate testing, tissue points within the dura and first 1 to 2 mm of the cortex could consistently be identified and tracked throughout the motion sequence, from initial acceleration up to impact speed and through the deceleration phase. Ultrasound images collected during low-rate testing also showed an interface layer visible between the dura and cortex. In Subject 1 and in pre-test trial subjects, this interface layer could be identified as the arachnoid using both anatomic location as well as relative tissue brightness compared to the underlying cortex in post-test images of the arachnoid taken with the dura removed. While the interface layer between the dura and cortex could not be definitively identified as the arachnoid in Subject 2 because of experimental issues that prevented post-test images with the dura removed, its anatomic location and its relative brightness compared to the underlying cortex did match typical post-test images of the arachnoid taken in previous subjects. Therefore, this layer will be assumptively labeled as the arachnoid$^\vee$ for the rest of the analysis, with the chevron flagging a level of uncertainty.

Sample tracking points on the dura, arachnoid$^\vee$, and near the cortical surface are shown in each image to illustrate how points in the tissue were tracked from frame to frame (Figure 8). Although for the purposes of illustration only one tissue point is shown in each layer of tissue in each of the frames shown, several tissue points were tracked across the width of each image frame for each layer of tissue. The retrograde configuration produced right-to-left motion in the image frame.
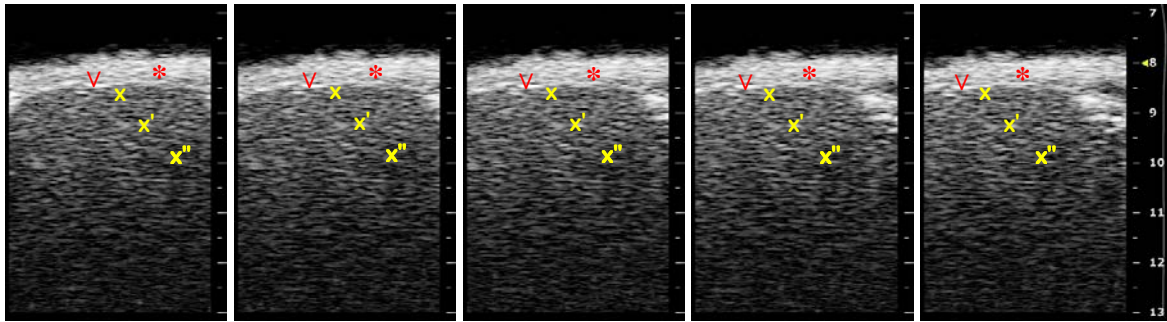
* - Dura

∨ - Arachnoid (point of chevron indicates tracked point)

x, x', xx" – Cortex, at increasing depth in tissue

Figure 8. Consecutive image frames prior to simulated impact (Subject 2, test LOW05) with a sample point tracked in each layer of tissue to illustrate tracking of tissue motion as head rotates past stationary transducer

Tissue points on the dura were tracked throughout the motion sequence to calculate cumulative lateral displacement of the dura past the ultrasound transducer, with correction for the spatio-temporal distortion that results from the sequential line-by-line image construction used in B-mode ultrasound (Figure 9). Peak error in cumulative displacement throughout the motion sequence *without* correction for spatio-temporal distortion would have been 1.4 mm, or approximately 7%.
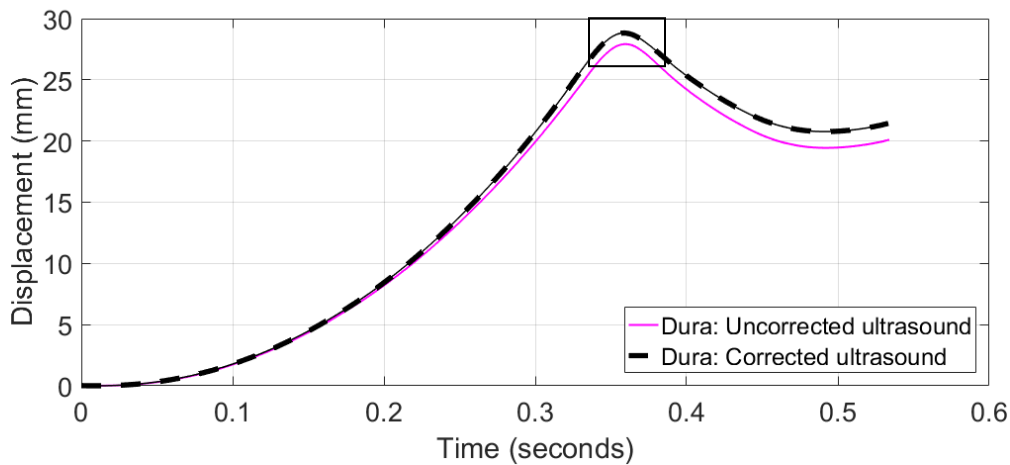
Figure 9. Cumulative displacement of dura throughout motion sequence before and after correction for spatio-temporal distortion, deceleration phase shown in box

Figure 10 and Figure 11 show the motion of the dura, the underlying arachnoid[∨], and the peripheral cortex during the deceleration phase marked with a box in Figure 9. The magnitude of the cumulative displacement on the Y-axis in Figure 10 reflects the total motion past the stationary ultrasound probe from the start of motion. The displacement peak corresponds to the timing of the head rotation being arrested by a padded brake stop, and the head bouncing back in the opposite direction. In Figure 11, cumulative displacement of the underlying layers is plotted relative to the dura, which was confirmed to be engaged with the skull during rotation. As in all of the low-rate testing on this subject, the tissue layer assumed to be the arachnoid had little or no motion relative to the dura, while the underlying cortex continued to move in the original direction of rotation when the skull was decelerated. In all low-rate testing, the cortex moved 0.1 to 0.2 mm farther than the dura and arachnoid[∨] during the deceleration pulse before returning to its initial position relative to the dura.
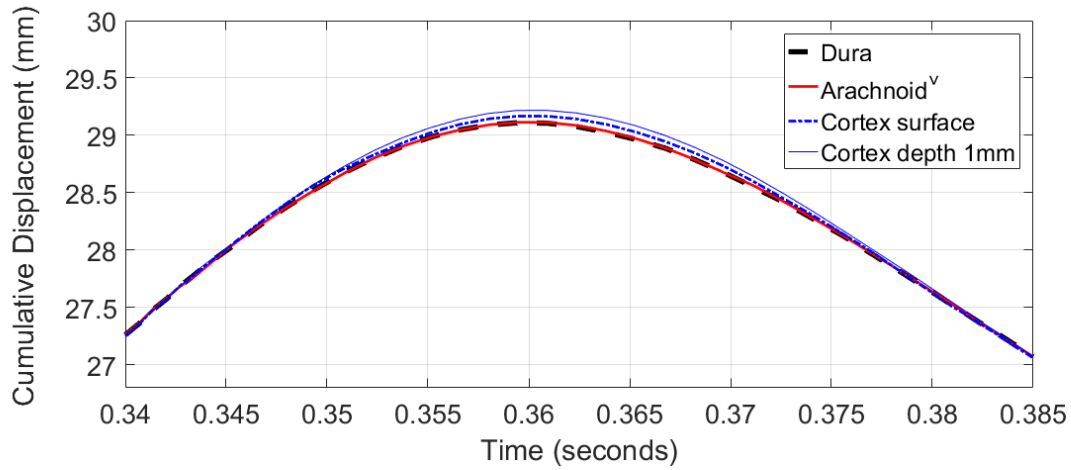
Figure 10. Cumulative displacement of peripheral tissue layers during rotation deceleration phase (corrected for spatio-temporal distortion)
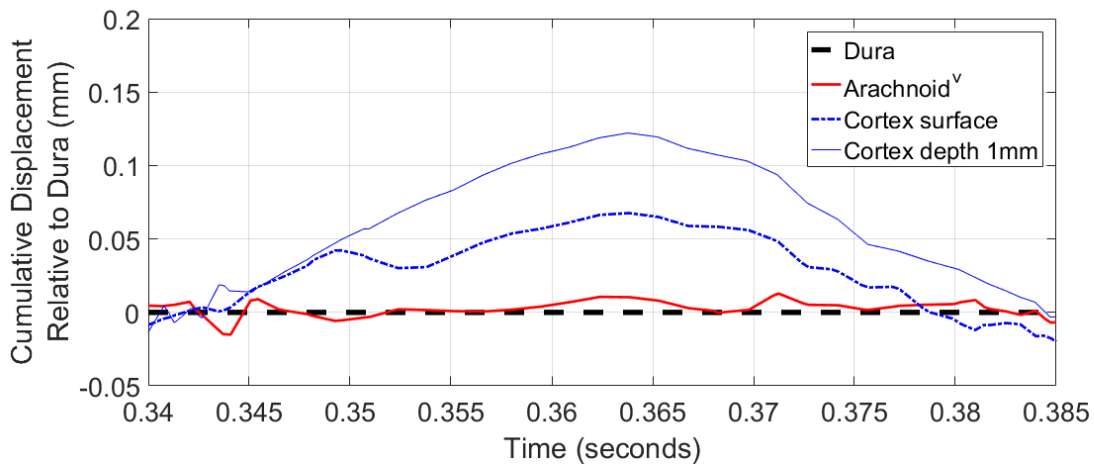
Figure 11. Cumulative displacement of arachnoid$^\vee$ and cortex relative to dura (all corrected for spatio-temporal distortion)

High-rate Results.   Ultrasound images were captured during high-rate rotation tests on both subjects. During a primary acceleration pulse of approximately 5 msec, the heads reached a peak rotational velocity, before decelerating to a steady-state velocity maintained for approximately 40 msec. Kinematic parameters measured are shown in Table 2 for two high-rate tests on Subject 2.

Table 2. Rotational Kinematics in High-Rate Tests

Test #	Peak Rotational Velocity	Steady State Rotational Velocity	Peak Rotational Acceleration	Primary Acceleration Duration
ROTATE02	21.4 rad/sec	15.5 rad/sec	7709 rad/sec^2	5 msec
ROTATE03	22.0 rad/sec	14.3 rad/sec	7717 rad/sec^2	5 msec

Ultrasound images in high-rate tests were of similar quality to those recorded in low-rate testing, allowing differentiation of tissue layers and visible identification of tissue features. However, tissue motion could not be tracked during the initial acceleration period in high-rate tests by either manual or semi-automatic methods because of outward bulging of the tissue resulting from radial acceleration. Since tracking is performed by registering the position of identifiable features on the tissue in consecutive frames, features must be visible for at least two consecutive frames in order to track frame-by-frame motion. In both subjects tested, radial bulging stretched and deformed the tissues out of the ultrasound imaging plane, such that individual points on the tissue could not be tracked from frame-to-frame during the primary acceleration period. In high-rate rotation tests with Subject 1, image frames in the primary acceleration period showed 1 to 2 mm of tissue motion toward the ultrasound probe. In Subject 2, efforts had been made to reduce axial motion by narrowing the lateral width of the window opening in the skull and buttressing the dura at the edges of the window with epoxy, reducing the radial bulging of the tissues to approximately 1 mm. However, individual points in each tissue layer still could not be identified in consecutive frames for tracking during the primary acceleration period in either subject, in spite of the fact that dura velocities were below the estimated 1.9 m/s maximum velocity where tissue features were expected to stay in view for at least 3 frames. As a result, motion tracking could not be performed on the high-rate tests in either subject.
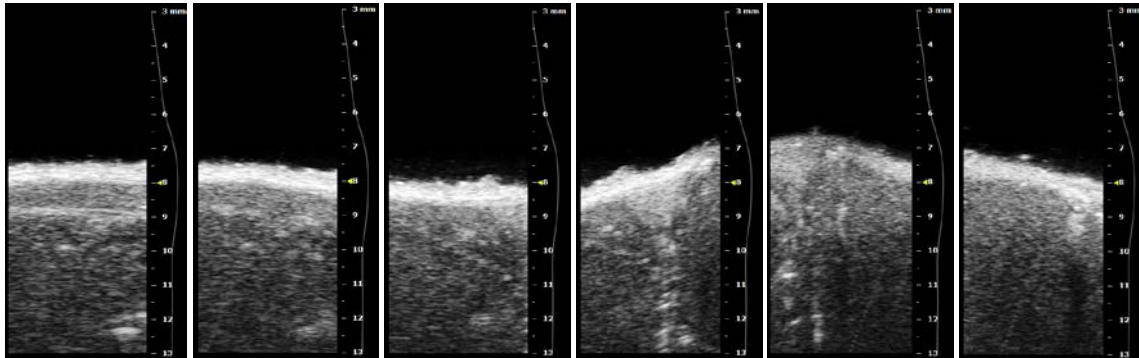
Figure 12. Consecutive ultrasound frames from initial acceleration in ROTATE02 in Subject 2.

DISCUSSION

The application of B-mode ultrasound holds promise for experimental biomechanics research that requires non-invasive tracking of tissue motion. While ultrafast ultrasonic imaging allows for higher-rate image collection than conventional B-mode ultrasound, better spatial resolution can be achieved with sequentially built B-mode images. For very small, 2-dimensional imaging areas, high-frequency B-mode ultrasound systems have the capability of imaging at resolutions of 80 μm or better, at up to 1000 frames per second (Visualsonics, 2009). Imaging wider or deeper areas with B-mode ultrasound can be achieved with compromises in spatial resolution and image frame rate.

In the current study of peripheral intracranial motion, B-mode ultrasound was successful at capturing the relative motion of the tissues at the surface of the brain during head rotation tests on two post-mortem human subjects. The dura, the surface of the cortex, and an intermediate layer believed to be the arachnoid were visualized and tracked throughout a motion sequence that simulated the head rotation experienced during a mild head impact. In all low-level head rotation tests performed in this study, ultrasound images were sufficient to identify negligible motion between the dura and arachnoid, and 1-2 mm of peripheral cortex motion relative to the arachnoid and dura. These displacements are consistent with the anatomical dural border cell layer connection between the dura and the arachnoid (Haines et al., 1993), and the tethering of the arachnoid to the cortex by the arachnoid trabeculae across the subarachnoid space. However, the magnitude of the relative motion measured should be interpreted as preliminary estimates, given that subject preparation techniques were still under development during the testing of these subjects. Damage to Subject 1's dura during preparation led to apparent fluid leakage between the dura and arachnoid.

Testing on Subject 2 was performed up to 86 hours post-mortem, a time delay known to result in mechanical changes to brain tissue properties (Stalnaker et al., 1977, Darvish et al., 2001, Nicolle et al., 2004, Bentil, 2013). Additionally, subject preparation techniques were still being improved during these tests, including vascular pressurization targeted at maintaining physiological levels of ICP and perfusion of the subarachnoid space with artificial CSF using extreme care to avoid breaching the arachnoid or introducing any fluid between the dura and arachnoid.

In higher-rate tests simulating trauma-level rotation of the head, individual images also showed sufficient resolution to visualize individual tissue layers. However, bulging of the tissue stretched the tissues in the viewing window such that motion of individual tissue points did not remain in the 2-dimensional ultrasound imaging plane. As a result, frame-by-frame motion of the dura, arachnoid, and cortex could not be tracked during the acceleration phase of head rotation, preventing measurement of relative motion of these layers. Tissue motion in the ultrasound viewing window will need to be kept in the plane of the ultrasound transducer in order to effectively track cumulative motion.

Solutions being explored to address the outward bulging of tissues include mounting the ultrasound transducer to the halo structure that rotates with the head. Fixing the transducer in place at the craniectomy location has several advantages over mounting it in a stationary position adjacent to the rotating head. Rotating the transducer with the head requires a much smaller craniectomy window, no larger than the face of the ultrasound array. An ultrasound gel pad can be inserted between the dura and the transducer and used as an imaging medium in place of a fluid pan. Not only can the much smaller craniectomy window reduce outward bulging during rotation but the transducer and gel pad also offer resistance to outward bulging, essentially replacing the removed skull at the craniectomy site. An additional benefit of mounting the ultrasound transducer on the rotating structure is a potential increase in the maximum tissue velocity that can be measured, since tissue will not be passing out of the ultrasound image window as quickly as it did for a transducer mounted in a stationary position adjacent to the head.

Preliminary rotation trials with a *halo-mounted* ultrasound transducer on a previously-frozen post-mortem human subject and on phantom tissues mounted in a rotating crash-test dummy head have been promising. Mounting the ultrasound transducer to the head, and imaging through a transducer-sized craniectomy has been confirmed to reduce bulging and preserve in-plane motion of the tissue at rotational acceleration rates up to 5000 rad/sec^2 and rotation speeds up to 30 rad/sec. In order to perform exploratory tests at higher rotation rates, ruggedization of the transducer mounting structure and tests to confirm the durability of the transducer are ongoing.

CONCLUSIONS

B-mode ultrasound has the potential to image internal tissue motion non-invasively in experimental biomechanics research. In low-rate post-mortem head rotation testing, high-frequency B-mode ultrasound was used to successfully track the relative motion of the dura and underlying tissues. Although tracking of the dura, arachnoid, and cortex was prevented in high-rate testing by out-of-plane motion of the tissues during rotation, the resolution of the images captured suggest that B-mode ultrasound has the potential to capture relative meningeal motion in trauma-level head rotation tests if outward bulging of the tissues and resulting out-of-plane motion can be reduced. Preliminary efforts to eliminate out-of-plane motion by mounting the ultrasound transducer to the structure that rotates with the head have been promising.

ACKNOWLEDGEMENTS

REFERENCES

BAYLY, P. V., COHEN, T. S., LEISTER, E. P., AJO, D., LEUTHARDT, E. C. and GENIN, G. M. (2005). Deformation of the human brain induced by mild acceleration. J Neurotrauma, 22, 845-856.

BEILLAS, P., HELFENSTEIN, C., RONGIERAS, F., GENNISSON, J. L. and TANTER, M. (2013). A new method to assess the deformations of internal organs of the abdomen during impact. Computer Methods in Biomechanics and Biomedical Engineering, 16, 202-203.

BENTIL, S. A. (2013). A fractional Zener constitutive model to describe the degradation of swine cerebrum with validation from experimental data and predictions using finite element analysis. Ph.D. Dissertation, Ohio State University.

DARVISH, K. and CRANDALL, J. (2001). Nonlinear viscoelastic effects in oscillatory shear deformation of brain tissue. Medical engineering & physics, 23, 633-645.

DEPREITERE, B., VAN LIERDE, C., SLOTEN, J. V., VAN AUDEKERCKE, R., VAN DER PERRE, G., PLETS, C. and GOFFIN, J. (2006). Mechanics of acute subdural hematomas resulting from bridging vein rupture. J Neurosurg, 104, 950-956.

FENG, Y., ABNEY, T. M., OKAMOTO, R. J., PLESS, R. B., GENIN, G. M. and BAYLY, P. V. (2010). Relative brain displacement and deformation during constrained mild frontal head impact. J R Soc Interface, 7, 1677-1688.

GENNARELLI, T. A. and GRAHAM, D. I. (2005). *Neuropathology*, in Textbook of Traumatic Brain Injury. J. M. Silver, T. W. McAllister and S. C. Yudofsky (eds). American Psychiatric Publishing, Inc. Washington, DC.

GENNARELLI, T. A. and THIBAULT, L. E. (1982). Biomechanics of acute subdural hematoma. J Trauma, 22, 680-686.

GOSCH, H. H., GOODING, E. and SCHNEIDER, R. C. (1970). The lexan calvarium for the study of cerebral responses to acute trauma. J Trauma, 10, 370-376.

HAINES, D. E., HARKEY, H. L. and AL-MEFTY, O. (1993). The "Subdural" Space: A New Look at an Outdated Concept. Neurosurgery, 32, 111-120.

HANIF, S., ABODUNDE, O., ALI, Z. and PIDGEON, C. (2009). Age Related Outcome in Acute Subdural Haematoma Following Traumatic Head Injury. Irish Medical Journal, 102, 255-257.

HARDY, W. N., MASON, M. J., FOSTER, C. D., SHAH, C. S., KOPACZ, J. M., YANG, K. H., KING, A. I., BISHOP, J., BEY, M., ANDERST, W. and TASHMAN, S. (2007). A study of the response of the human cadaver head to impact. Stapp Car Crash J, 51, 17-80.

HELFENSTEIN-DIDIER, C., TANTER, M., GENNISSON, J.-L. and BEILLAS, P. (2015). Observation of the internal response of the kidney during compressive loading using ultrafast ultrasonography. Journal of biomechanics, 48, 1852-1859.

HODGSON, V. R., GURDJIAN, E. S. and THOMAS, L. M. (1966). Experimental skull deformation and brain displacement demonstrated by flash x-ray technique. J Neurosurg, 25, 549-552.

HOLBOURN, A. H. S. (1943). Mechanics of Head Injuries. Lancet, 2, 438-441.

IBRAHIM, N. G., NATESH, R., SZCZESNY, S. E., RYALL, K., EUCKER, S. A., COATS, B. and MARGULIES, S. S. (2010). In situ deformations in the immature brain during rapid rotations. J Biomech Eng, 132, 044501.

JAMIESON, K. G. and YELLAND, J. D. (1972). Surgically treated traumatic subdural hematomas. J Neurosurg, 37, 137-149.

JI, S., ZHU, Q., DOUGHERTY, L. and MARGULIES, S. S. (2004). In vivo measurements of human brain displacement. Stapp Car Crash J, 48, 227-237.

KING, A. I., RUAN, J. S., ZHOU, C., HARDY, W. N. and KHALIL, T. B. (1995). Recent Advances in Biomechanics of Brain Injury Research: A Review. Journal of Neurotrauma, 12, 651-658.

KLEIVEN, S. and VON HOLST, H. (2002). Consequences of head size following trauma to the human head. J Biomech, 35, 153-160.

LÖWENHIELM, P. (1974). Strain tolerance of the vv. cerebri sup. (bridging veins) calculated from head-on collision tests with cadavers. Z Rechtsmed, 75, 131-144.

MALLORY, A. (2010). Head injury and aging: the importance of bleeding injuries. Ann Adv Automot Med, 54, 51-60.

MALLORY, A., HERRIOTT, R. and RHULE, H. (2011). Subdural Hematoma and Aging: Crash Characteristics and Associated Injuries. 22nd International Technical Conference on the Enhanced Safety of Vehicles (ESV), Paper Number 11-0399.

MALLORY, A. E. (2014). Measurement of Meningeal Motion Using B-Mode Ultrasound as a Step Toward Understanding the Mechanism of Subdural Hematoma. PhD Dissertation, The Ohio State University.

MARGULIES, S. S., THIBAULT, L. E. and GENNARELLI, T. A. (1990). Physical model simulations of brain injury in the primate. J Biomech, 23, 823-836.

MAXEINER, H. (1997). Detection of ruptured cerebral bridging veins at autopsy. Forensic Sci Int, 89, 103-110.

MAXEINER, H. and WOLFF, M. (2002). Pure Subdural Hematomas: A Postmortem Analysis of Their Form and Bleeding Points. Neurosurgery, 50, 503-509.

MEANEY, D. F. (1991). Biomechanics of acute subdural hematoma in the subhuman primate and man. PhD Dissertation, University of Pennsylvania.

NICOLLE, S., LOUNIS, M. and WILLINGER, R. (2004). Shear Properties of Brain Tissue over a Frequency Range Relevant for Automotive Impact Situations: New Experimental Results. Stapp Car Crash Journal, 48, 239.

NUSHOLTZ, G. S., LUX, P., KAIKER, P. and JANICKI, M. A. (1984). Head Impact Response - Skull Deformation and Angular Accelerations. Stapp Car Crash Conference, Society of Automotive Engineers: 41-74.

OMMAYA, A. K., FAAS, F. and YARNELL, P. (1968). Whiplash injury and brain damage: an experimental study. JAMA, 204, 285-289.

OMMAYA, A. K., GOLDSMITH, W. and THIBAULT, L. (2002). Biomechanics and neuropathology of adult and paediatric head injury. British Journal of Neurosurgery, 16, 220-242.

PEREL, P., ROBERTS, I., BOUAMRA, O., WOODFORD, M., MOONEY, J. and LECKY, F. (2009). Intracranial bleeding in patients with traumatic brain injury: A prognostic study. BMC Emergency Medicine, 9, 15.

PUDENZ, R. H. and SHELDEN, C. H. (1946). The lucite calvarium; a method for direct observation of the brain; cranial trauma and brain movement. J Neurosurg, 3, 487-505.

RABOEL, P., BARTEK, J., ANDRESEN, M., BELLANDER, B. and ROMNER, B. (2012). Intracranial pressure monitoring: invasive versus non-invasive methods—a review. Critical Care Research and Practice, 2012.

SABET, A. A., CHRISTOFOROU, E., ZATLIN, B., GENIN, G. M. and BAYLY, P. V. (2008). Deformation of the human brain induced by mild angular head acceleration. Journal of Biomechanics, 41, 307-315.

SASS, D. J., CORRAO, P. and OMMAYA, A. K. (1971). Brain motion during vibration of water immersed rhesus monkeys. J Biomech, 4, 331-334.

SAWAUCHI, S. and ABE, T. (2008). The effect of haematoma, brain injury, and secondary insult on brain swelling in traumatic acute subdural haemorrhage. Acta Neurochir (Wien), 150, 531-536.

SHATSKY, S. A., ALTER, W. A., III, EVANS, D. E., ARMBRUSTMACHER, V. and CLARK, G. (1974). Traumatic Distortions of the Primate Head and Chest: Correlation of Biomechanical, Radiological and Pathological Data. Stapp Car Crash Conference, Society of Automotive Engineers**:** 351-381.

SHELDON, C. H., PUDENZ, R. H., RESTARSKI, J. S. and CRAIG, W. M. (1944). The lucite calvarium - a method for direct observation of hte brain. I. The surgical and lucite processing techniques. Journal of Neurosurgery 1, 67-75.

STALNAKER, R. L., MELVIN, J. W., NUSHOLTZ, G. S., ALEM, N. M. and BENSON, J. B. (1977). Head Impact Response. Stapp Car Crash Conference, Society of Automotive Engineers**:** 305-335.

STITZEL, J. D., KILGO, P. D., DANELSON, K. A., GEER, C. P., PRANIKOFF, T. and MEREDITH, J. W. (2008). Age thresholds for increased mortality of three predominant crash induced head injuries. Annu Proc Assoc Adv Automot Med, 52, 235-244.

SUGAWARA, O., ATSUTA, Y., IWAHARA, T., MURAMOTO, T., WATAKABE, M. and TAKEMITSU, Y. (1996). The effects of mechanical compression and hypoxia on nerve root and dorsal root ganglia. An analysis of ectopic firing using an in vitro model. Spine, 21, 2089-2094.

TAUSSKY, P., WIDMER, H. R., TAKALA, J. and FANDINO, J. (2008). Outcome after acute traumatic subdural and epidural haematoma in Switzerland: a single-centre experience. Swiss Med Wkly, 138, 281-285.

TROSSEILLE, X., TARRIÉRE, C., LAVASTE, F., GUILLON, F. and DOMONT, A. (1992). Development of a F.E.M. of the Human Head According to a Specific Test Protocol. Stapp Car Crash Conference, 235-253.

VIANO, D., ALDMAN, B., PAPE, K., VAN HOOF, J. and VON HOLST, H. (1997). Brain kinematics in physical model tests with translational and rotational acceleration. International Journal of Crashworthiness, 2, 191-205.

VISUALSONICS (2009). Vevo2100 Transducers v1.9. VisualSonics. Toronto, Ontario.

YAMASHIMA, T. and FRIEDE, R. L. (1984). Why do bridging veins rupture into the virtual subdural space? J Neurol Neurosurg Psychiatry, 47, 121-127.

All Authors full name, address and E-mail

1. Ann Mallory
2. Transportation Research Center Inc.
   10820 State Route 347
   East Liberty, Ohio   43319-0337
3. Phone: 937-666-3235 Fax: 937-666-3590
4. ann.mallory.ctr@dot.gov

1. Rodney G. Herriott*
2. Formerly of Transportation Research Center Inc.
   *Deceased prior to final submission of manuscript

1. Yun-Seok Kang
2. Injury Biomechanics Research Center
   333 West 10th Ave, RM2063
   Columbus, Ohio 43210
3. Phone: 614-366-7584, Fax : 614-292-7659
4. yunseok.kang@osumc.edu

1. Heather Rhule
2. Vehicle Research and Test Center, National Highway Traffic Safety Administration
   10820 State Route 347
   East Liberty, Ohio   43319-0337
3. Phone: 937-666-4511 Fax: 937-666-3590
4. Heather.rhule@dot.gov

1. Bruce Donnelly
2. 22 West Lincoln Avenue
   Delaware, Ohio   43015
3. Phone: 740-363-6230
4. brucedonnellyphd@columbus.rr.com

1. Kevin Moorhouse
2. Vehicle Research and Test Center, National Highway Traffic Safety Administration
   10820 State Route 347
   East Liberty, Ohio   43319-0337
3. Phone: 937-666-4511 Fax: 937-666-3590
4. Kevin.moorhouse@dot.gov